Research Article

Magneto-structural and induction heating properties of MFe_2O_4 (M = Co, Mn, Zn) MNPs for magnetic particle hyperthermia application

Anil Salokhe[1] · Amruta Koli[1] · Vidhya Jadhav[1] · Shubhangi Mane-Gavade[1] · Amit Supale[3] · Rohant Dhabbe[1] · Xiao-Ying Yu[2] · Sandip Sabale[1,2]

Received: 12 August 2020 / Accepted: 9 November 2020 / Published online: 19 November 2020

Abstract
The complex decomposition approach was used for the synthesis of MFe_2O_4 magnetic nanoparticles (MNPs) by substituting M as Co, Mn, and Zn. The obtained MNPs were characterized for magneto-structural properties using X-Ray diffraction patterns, FTIR, Raman and Mossbauer spectroscopy techniques which validate the synthesis of phase pure cubic spinel ferrite (space group *Fd3m*) with five Raman active modes. Magnetic properties confirmed using Mossbauer spectroscopy. The size, morphology, and compositional analysis was performed using HRTEM and EDX where the size of MNPs was found to be less than 10 nm that attains superparamagnetism with 39.0, 58.28, and 44.24 emu gm^{-1} moment for $CoFe_2O_4$, $MnFe_2O_4$, and $ZnFe_2O_4$, respectively. The magnetic hyperthermia performance of obtained MNPs was evaluated by induction heating experiments at magnetic field range 13.3–26.7 kAm^{-1}. The specific absorption rate (SAR) and intrinsic loss power (ILP) values were determined at different magnetic fields and mutually related with magneto-structural properties to evaluate its potential for magnetic particle hyperthermia therapy. The $CoFe_2O_4$ MNP exhibits a maximum temperature rise of 25 and 35 °C for 5 and 10 $mgmL^{-1}$ concentrations with threshold temperature rise.

Keywords Complex decomposition · Magnetic nanoparticles · Magneto-structural properties · Magnetic fluid hyperthermia (MFH) · Saturation magnetization

1 Introduction

The use of magnetic nanoparticles (MNPs) has interestingly increased due to its application in many fields such as magnetic storage, catalysis, photocatalysis, sensor, and biomedical applications [1–5]. In recent days, the MNPs are the best option in various biomedical fields like cancer treatment by magnetic fluid hyperthermia (MFH), targeted drug delivery, bioimaging, bioseparation, and biosensor [6–10]. Many researchers have reported that MFH is an alternative technique for cancer treatment without damaging normal cells as in chemotherapy. There have been different classes of MNPs, namely, metals, metal oxides (Fe_2O_3, Fe_3O_4, Mn_3O_4), ferrites (MFe_2O_4), and alloys [11–15]. Ferrites (MFe_2O_4) are much more influential MNPs among others due to its simple synthetic process, distinctive chemical properties, biocompatibility and non-toxicity to human, controllable size, dispersibility and magnetism for manipulation with an external magnetic field, and these features make them potentially applicable in the biomedical fields [9, 16–19]. The doping of metal ions shows superlative effect in physicochemical properties, stability

Electronic supplementary material The online version of this article (https://doi.org/10.1007/s42452-020-03865-x) contains supplementary material, which is available to authorized users.

✉ Sandip Sabale, srsabale@gmail.com | [1]Department of Chemistry, Jaysingpur College Jaysingpur, Jaysingpur, Maharashtra 416101, India. [2]Energy and Environment Directorate, Pacific Northwest National Laboratory, Richland, WA 99354, USA. [3]Department of Chemistry, Dr. Patangrao Kadam Mahavidyalaya, Sangli, Maharashtra 416416, India.

toward the seepage of Fe ions and notable improvement in biocompatibility and magnetic properties [8, 19–21]. Furthermore, the physical and chemical properties of ferrite MNPs mainly depend on the uniformity of particle size, shape, and stability, so it is of ample importance to prepare MNPs with controllable morphology, size, and good stability. Considering these factors, researchers nowadays are interested in tuning the properties of MNPs by doping with metal ions to control particle size, magnetization, morphology, and rise in temperature by induction heating using an external magnetic field to explore these MNPs as MFH [22, 23]. The rise in temperature in such induction heating studies should be expected between 41 °C–46 °C so as to discard the cancer cells which can be achieved by doping the ferrites with metal ions [22]. Additionally, specific absorption rate (SAR) and intrinsic loss power (ILP) are crucial aspects in this technique of MFH where higher SAR and ILP value bearing MNPs are expected within the human tolerance limit of frequency and amplitude that of the external magnetic field to treat cancer via MFH [7, 24]. Another way to achieve the desired properties of MNPs is synthesis methods where different methods have been employed including but not limited to precipitation, sol–gel, microemulsion, complex decomposition, hydrothermal, and solvothermal method [25]. Among these methods, the complex decomposition method mainly used to obtain monodispersed MNPs with monodispersibility, narrow size distribution and controllable size (below 10 nm) and morphologies due to which they own superparamagnetism [26–28].

In this work, we report the synthesis of $CoFe_2O_4$, $MnFe_2O_4$, and $ZnFe_2O_4$ MNPs using the complex decomposition method to investigate the change in magnetic and structural properties using M-H curves, X-Ray diffraction (XRD), FTIR, Raman, and Mossbauer spectroscopy. The obtained MNPs were also explored in induction heating studies within the human tolerable range from which values related to SAR and ILP have been calculated to characterize their applicability and potential in MFH for cancer treatment.

2 Experimental

For the synthesis of MNPs, analytical research (AR) grade cobalt (Co, II) acetylacetonate ($Co[acac]_2$, 97%), manganese (Mn, II) acetylacetonate ($Mn[acac]_2$, 97%), zinc (Zn, II) acetylacetonate ($Zn[acac]_2$, 97%), and iron (Fe, III) acetylacetonate ($Fe[acac]_3$, 97%) were purchased from Sigma-Aldrich. Diethylene glycol (99.5%) and ethylene glycol (99.5%) of AR grade were purchased from Thomas Baker while oleylamine (98%) and oleic acid (69%) were purchase from Sd-Fine and Fisher Scientific, respectively; and all these chemicals were used as received.

2.1 Synthesis of MFe_2O_4 MNPs

$Co/Mn/ZnFe_2O_4$ MNPs were synthesized using the complex decomposition method reported in our previous work [29]. Briefly, metal precursors of Co/Mn/Zn (2 mmol) are mixed separately in a solution of $Fe(acac)_3$ in a mixture of diethylene glycol and ethylene glycol (10 mL each) containing oleylamine and oleic acid (6 mmol each) followed by purging with N_2 at 120 °C for 10 min. Then, the whole solution was refluxed at 120 °C for 2 h. The as-prepared MNPs were then separated by adding 20 mL ethanol followed by centrifugation. The obtained $Co/Mn/ZnFe_2O_4$ MNPs were washed with hexane/ethanol (1:1 v/v) mixture (3×10 mL) and finally dispersed in hexane. The powder for characterization was obtained by washing with ethanol and drying in air. Obtained MNPs were characterized using different techniques and were used in induction heating studies.

2.2 Characterization of MNPs

UV/visible and FTIR spectra of synthesized MNPs were obtained using a UV/Vis/NIR (V-770, Jasco, Japan) spectrophotometer and FTIR spectrometer (4600 LE, Jasco, Japan). XRD patterns were recorded using X'pert PRO (Philips Eindhoven Netherlands) X-ray diffractometer (CuK radiation line $\lambda = 1.5406$ Å; 40 kV/40 mA). The elemental composition was obtained from energy-dispersive x-ray spectrometer (EDS) (JEOL JSM 5600), and the Raman spectra were recorded using a micro-Raman spectrometer (Horiba; JobinVyon) at 488 nm excitation laser 1800 gmm^{-1} grating with a CCD detector. HRTEM images were obtained using TEM-JEM-2100 (JEOL) operated at 200 kV. The magnetic properties (M-H curves) were determined using an alternating gradient magnetometer (AGM) (Micromeg Tm 2900, PMC). Mossbauer measurements were recorded using the Weissel velocity drive operating in the constant acceleration mode at room temperature.

2.3 Induction heating experiment

Induction heating studies of obtained MNPs were made using Easy Heat 8310, Ambrell, UK with 6 cm diameter coil (4 turns) with water circulation for ambient temperature. For this study, the suspended aqueous sample (5 and10 mg/mL) is taken in a plastic micro-centrifuge tube placed at the center of the coil under the applied frequency 276 kHz. The temperature rise experiments were recorded for 20 min. with 1 min. increment at the applied magnetic field (H) of 13.3, 20.0 and 26.7 kAm^{-1}. The optical

fiber probe system with an accuracy 0.1 °C was used for measuring temperature rise throughout the experiment. The heating ability of the MNPs and its potential to use for cancer hyperthermia treatment under the AC magnetic field was measured in terms of SAR and ILP values.

3 Results and discussion

3.1 Magneto-structural properties of MNPs

The characterization of obtained MNPs was performed using XRD analysis for the investigations of structural properties. The XRD patterns of $CoFe_2O_4$ (red) $MnFe_2O_4$ (blue) and $ZnFe_2O_4$ (green) MNPs are given in Fig. 1A. The diffraction peaks having 2θ values 30.16°, 35.34°, 42.97°, 56.31°, and 62.41°, corresponds to the peak indices 220, 311, 400, 333, and 440, respectively, was reveled from XRD pattern of MNPs; while the purity and phase of the obtained ferrites were confirmed with the absence of peaks at 210 and 300. The validation regarding the formation of a cubic spinel ferrite (space group *Fd3m*) was also done from XRD patterns. Scherer's formula [13] was used to determine crystallite sizes and were calculated by considering full width at half-maximum (FWHM) of peak in each sample corresponding indices of 311. The values of d-spacing, lattice constant (a), X-ray density (D_X), surface area (S), volume (a^3) have been also determined from the XRD patterns and reported in Table 1. From these values, it is determined that less than 10 nm size MNPs with the high surface area can be obtained using the complex decomposition method. The different absorption bands in FTIR spectra (Fig. 1B) support formation of spinel ferrite [30, 31]. For the synthesized MNPs, metal-oxide vibrational stretch in the spinel ferrite corresponding to the Fe–O and Co–O shows intense and broad absorption band at ~ 547 cm^{-1} [32]. The broad absorption band at ~ 3390 cm^{-1} corresponds to surface –OH or –NH stretching vibrations while the intense bands at 1062, 1409, and 1550 cm^{-1} correspond to –CO vibration, COO^- symmetric and asymmetric stretching, respectively. The bands at 2852 and 2922 cm^{-1} represent the symmetric and asymmetric stretching of $–CH_2$, indicating the presence of adsorbed oleic acid-oleylamine on the surface of the MNPs (Fig. 1B) [31]. In the present study, the MNPs were also characterized using Raman spectroscopy to find out additional information about the coordination of the metal ions in obtained MFe_2O_4 as it is a versatile tool for investigating the purity of spinel ferrites (MFe_2O_4). $CoFe_2O_4$, $MnFe_2O_4$, and $ZnFe_2O_4$ confirmed a cubic spinel structure that belongs to the space group O_h^7 (*Fd3m*). Total 42 vibrational modes are possible in such structures while five Raman active modes were predicted from the factor group analysis are $A_{1g} + E_g + 3T_{2g}$. The Raman spectra of obtained MNPs in a frequency range of 150–1000 cm^{-1}

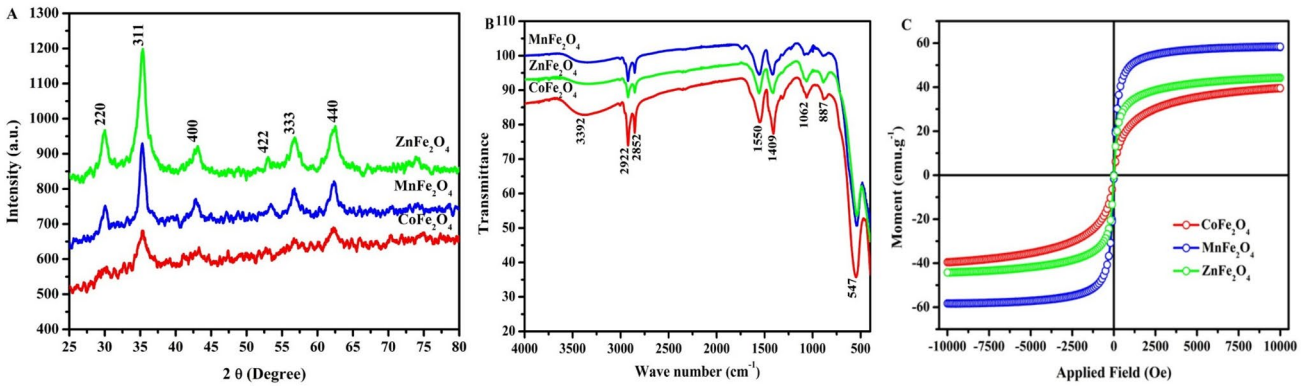

Fig. 1 X-Ray diffraction patterns **(A)**; FTIR spectra **(B)** and MH curves **(C)** of obtained $CoFe_2O_4$ (red), $MnFe_2O_4$ (blue), and $ZnFe_2O_4$ (green) MNPs

Table 1 Crystallite size obtained from XRD (D_{XRD}), TEM diameter (D_{TEM}), *d*-spacing, lattice constant (a) X-ray density (D_X), surface area (S), volume (a^3) and EDS composition of obtained MNPs

MNPs	D_{XRD} (nm)	D_{TEM} (nm)	d-spacing	'a' (Å)	D_X ($g.cm^{-3}$)	S ($m^2 \cdot g^{-1}$)	a^3 (cm^3) × 10^{-24}	Composition (wt %)		
								O	Fe	M
$CoFe_2O_4$	5.6 ± 1.0	4.0 ± 1.0	2.5349	8.4073	5.244	237.85	594.25	21.87	50.75	27.37
$MnFe_2O_4$	6.8 ± 1.3	6.0 ± 1.0	2.5410	8.4275	5.179	142.68	598.54	32.58	51.32	16.09
$ZnFe_2O_4$	7.1 ± 2.5	6.0 ± 1.0	2.5486	8.4527	5.160	110.31	603.93	28.49	49.48	22.03

are shown in Fig. 2. It is observed that the modes above 600 cm^{-1} are of the A_{1g} type, involving the symmetric stretching of O in tetrahedral AO_4 groups (A = Fe, Mn, Zn, Co). From the data obtained from Raman spectroscopy (Fig. 2A), the MNPs of $CoFe_2O_4$ show Raman active bands near 296 cm^{-1}, 459 cm^{-1}, and 672 cm^{-1}which are also supported from literature data. The characteristic intense band at 672 cm^{-1} (682 cm^{-1}) and 459 cm^{-1} (470 cm^{-1}) is corresponds to the A_{1g} symmetry of tetrahedral and octahedral site, respectively, which indicates the absence of magnetite, hence confirming the phase purity of $CoFe_2O_4$ [17, 33, 34]. Similarly, the other low-frequency modes in $MnFe_2O_4$ (Fig. 2B) and $ZnFe_2O_4$ (Fig. 2C) represent the characteristics of the octahedral sites [35, 36]. The presence of high purity spinel ferrites was further supported by absence of impurity related Raman active modes (ferrihydrite phase) at 710 and 1320 cm^{-1} [35].

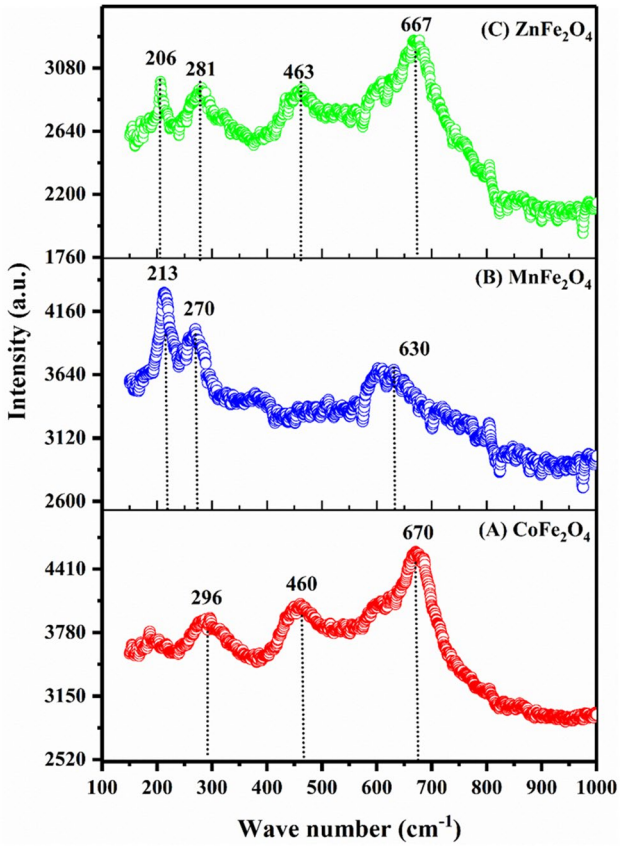

Fig. 2 Raman spectra showing the Raman active bands excited at 588 nm of obtained $CoFe_2O_4$ **(A)**, $MnFe_2O_4$ **(B)**, and $ZnFe_2O_4$ **(C)** MNPs

The magnetic properties of the MNPs were determined from M-H curves (Fig. 1C) illustrate that the saturation magnetization (M_S) obtained for $CoFe_2O_4$, $MnFe_2O_4$, and $ZnFe_2O_4$ NPs was 39.0, 58.28, and 44.24 $emug^{-1}$, respectively, with zero or negligible remanence or coercivity (H_C) which depicts the superparamagnetic behavior. The obtained values of magnetic properties are given in Table 2. In addition, the ^{57}Fe Mossbauer measurements with constant acceleration mode were conducted to determine the magneto-structural effect of M^{2+} variation on MNPs. Very broad Mossbauer spectra for all the 3 synthesized MNPs samples, indicates the distribution of hyperfine fields. Hence, the data were analyzed with the distribution of hyperfine fields using the NORMOS/DIST program as shown in Fig. 3 and the hyperfine parameters obtained are given in Table 2. Figures 3A–C show a similar FWHM (0.45 mms^{-1}) for obtained MNPs using fit hyperfine distribution. While the $CoFe_2O_4$ and $MnFe_2O_4$ MNPs show sextet which is a characteristic property of the superparamagnetism for both types of MNPs [37–39]. On the other hand, $ZnFe_2O_4$ had a doublet with an average isomer shift of 0.346 mms^{-1} which is the characteristic property of $ZnFe_2O_4$ as expected. It also showed a low average internal hyperfine field (H_f) when compared to $CoFe_2O_4$ and $MnFe_2O_4$ MNPs, and this closely resembles findings in the literature [31, 40, 41]. The relaxation effects showed a broad hyperfine distribution with a sextet in Mossbauer analysis due to the existence of fine nanoparticle size with strong interparticle interactions and high magnetization excluding $ZnFe_2O_4$. The HRTEM micrographs shown in Fig. 3D–F supports the aggregation of particles. The HRTEM results showed a quasi-spherical morphology with a size of 4 ± 1, 6 ± 1, and 6 ± 1 nm for $CoFe_2O_4$, $MnFe_2O_4$, and $ZnFe_2O_4$, respectively, is obtained by complex decomposition method and these sizes are consistent with the crystallite sizes obtained from XRD patterns. The compositional analysis determined by EDS is given in Table 1 which shows the existence of Fe and O along with Co, Mn, and Zn

Table 2 Saturation magnetization (M_S), coercivity (H_C) and magnetic moment (μ_B) obtained from MH curves; full width half maxima (FWHM), average isomer shift (I_S) and average internal hyperfine field (H_f) obtained from Mossbauer analysis of obtained MNPs

MNPs	M_S ($emug^{-1}$)	H_C (Oe)	μ_B	FWHM (mms^{-1})	I_S (mms^{-1})	H_f (mms^{-1})
$CoFe_2O_4$	39.0	0.0	1.6384	0.45	0.328	26.6
$MnFe_2O_4$	58.28	2.58	2.3760	0.45	0.336	30.9
$ZnFe_2O_4$	44.24	0.63	1.9096	0.45	0.346	7.43

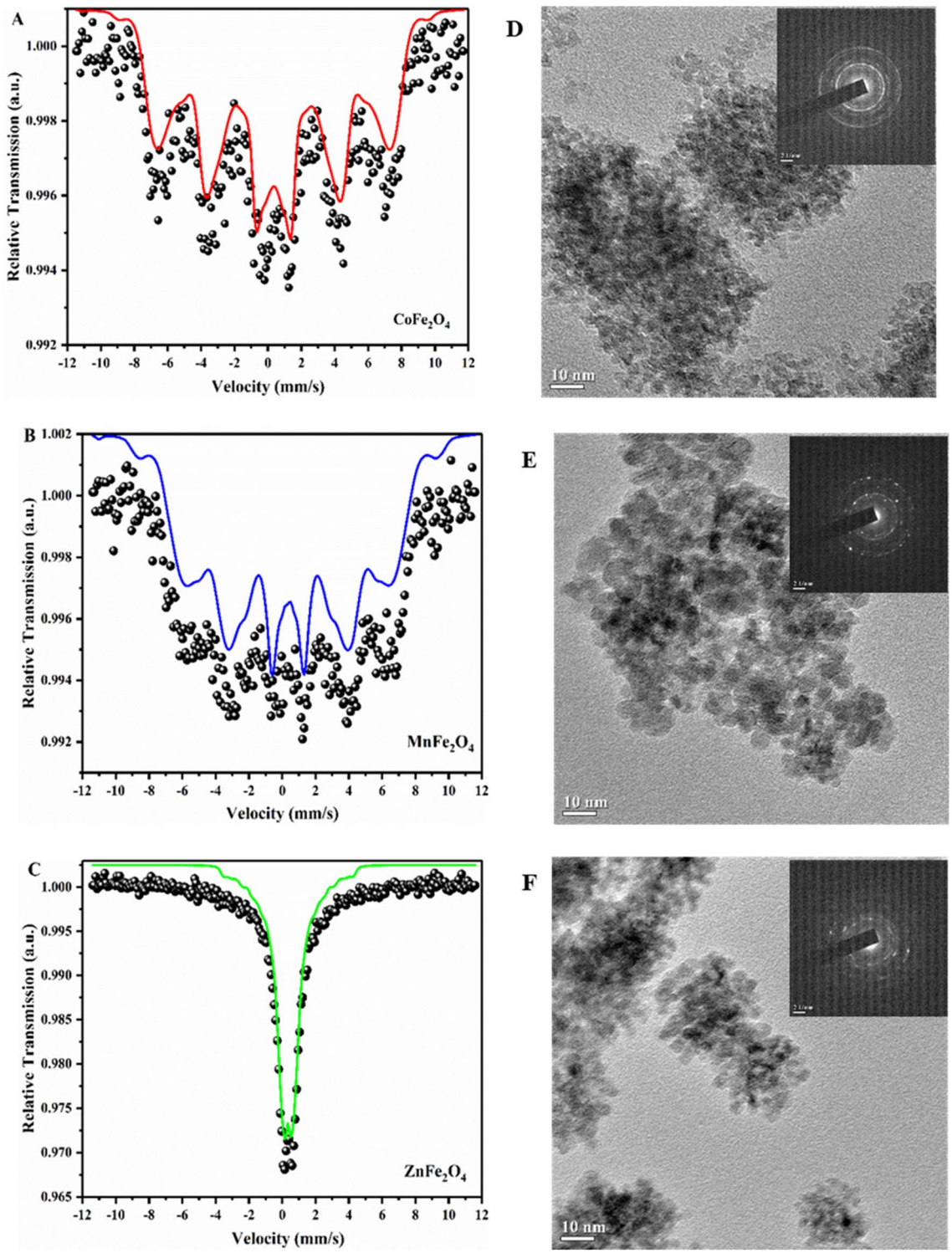

Fig. 3 Room temperature Mossbauer spectra (**A**, **B** and **C**) and TEM micrographs (**D**, **E** and **F**) of $CoFe_2O_4$, $MnFe_2O_4$, and $ZnFe_2O_4$ MNPs, respectively. Inset shows the SAED patterns correspond to XRD patterns

in respective MNPs. From these results, it is observed that 22% of Fe is replaced by Zn in the case of $ZnFe_2O_4$, while 27.37% of Fe is replaced by less magnetic Co (compared to Fe) in $CoFe_2O_4$, which influenced directly on its saturation magnetization *Ms*. Hence $CoFe_2O_4$ showed low *Ms* than $ZnFe_2O_4$. Our results support the formation of the phase

pure cubic spinel structured superparamagnetic $CoFe_2O_4$, $MnFe_2O_4$, and $ZnFe_2O_4$ NPs.

3.2 Induction heating studies and determination of SAR and ILP values

The magnetic hyperthermia performance of the obtained $CoFe_2O_4$, $MnFe_2O_4$, and $ZnFe_2O_4$ MNPs was estimated by induction heating as per the experimental procedure. The studies on effect of MNPs concentration and field parameters on self-heating temperature rise properties are carried out. The factual increment in temperature in a time span of 1200 s. for the MFe_2O_4 was determined at two different MNP concentrations (5 and 10 mg/mL) at various magnetic field (13.3, 20.0 and 26.7 kAm^{-1}) (Figs. 4A–F). The graphs show a linear relationship of temperature with applied field amplitude. Generally, 41–46 °C temperature is considered as effective for hyperthermia therapy [22]. Observed rapid temperature rise in the initial stages can be attributed to the magnetic hysteresis loss when Neel and Brownian relaxations of each ferrimagnetic nanoparticles are activated by the magnetic field [22, 23].

From Fig. 4, it is observed that the time needed to reach the expected hyperthermia temperature for the MNPs with a concentration 10 $mgmL^{-1}$ is less than that of the MNPs with a concentration of 5 $mgmL^{-1}$; and the time duration varies as a function of the applied field. It is clear that with an increase in particle concentration there will be more MNPs in the increased particle–particle interactions, which increases the exchange coupling energy and affects the induction heating [19, 42].

$CoFe_2O_4$ MNPs were capable to produce sufficient threshold heat rise expected for effective MFH for both 5 and 10 $mgmL^{-1}$ MNP concentrations above 13.3 kAm^{-1} applied field (Figs. 4A, B). Here, $MnFe_2O_4$ MNPs (5 and 10 $mgmL^{-1}$) are fail to produce sufficient heat rise up to the 20 kAm^{-1} field while at 26.7 kAm^{-1} it showed sufficient induction heating required for hyperthermia. However, $ZnFe_2O_4$ MNPs are impotent to achieve temperature rise for both the concentrations. This large discrepancy in the heat generation from the similar mass of sample suggests that the magneto-structural properties of the MNPs are also of importance along with the field parameters [19, 43]. The synthesized MNPs should exhibit a maximum heating temperature (ΔT_{max}), to overcome the loss in temperature rise due to blood circulation and tissue perfusion, The T_{max} is higher for 10 $mgmL^{-1}$ than 5 $mgmL^{-1}$ concentrations for all samples (Fig. 5). The $CoFe_2O_4$ MNP exhibits a maximum temperature rise of 25 and 35 °C for 5 and 10 $mgmL^{-1}$ concentrations. The maximum temperature rise for $MnFe_2O_4$ was found to be 13 and 17 °C for 5 and 10 $mgmL^{-1}$; while in the case of $ZnFe_2O_4$ it is 11 and 13 °C. This result indicates that heat generation ability depends on various factors such as crystallite size, structural factors such as anisotropy, shape, particle size distribution, agglomeration, interparticle interaction as well as susceptibility/permeability of the materials [4].

The heat loss generated by MNPs in the alternating magnetic field is estimated from specific absorption rate (SAR) values and was calculated from Eq. (1).

$$\mathrm{SAR} = C\,X\left(\frac{\mathrm{d}T}{\mathrm{d}t}\right)X\left(\frac{m_s}{m_m}\right) \tag{1}$$

where C = specific heat capacity of suspension = 4.186 J $(g\,°C)^{-1}$, (dT/dt) = initial slope of temperature versus time graph, m_s = mass of suspension, and m_m = mass of the magnetic material in suspension. These SAR values should be as high as possible to minimize the amount of magnetic material used for hyperthermia. The SAR values of the MFe_2O_4 samples are calculated and plotted as a function of the applied field and particle concentration (Fig. 6).

As mentioned in our earlier report [29], the heating abilities of the single-particle are attributed to the power loss caused by hysteresis and relaxation losses for single domain NPs. In superparamagnetic NPs, the power loss is the root of only relaxations which are attributed due to the Neel and Brown relaxations which are major contributors to the SAR values. These losses in the AC magnetic field can be expressed as [24],

$$A = \int_{-H_{min}}^{-H_{max}} \mu_0 M(H)\mathrm{d}H \tag{2}$$

Hence, SAR becomes,

$$\mathrm{SAR} = \mathrm{A\,f} \tag{3}$$

where, f is the frequency of magnetic field, M magnetization, and H the applied magnetic field. Thus, SAR dependence on the frequency and amplitude of magnetic field is accountable in such studies as a human acceptable range of frequency and amplitude is considered to be $f < 1.2$ MHz and $H < 15$ kAm^{-1}, respectively. The tolerable value is expressed in terms of C which is given by $(f \times H)$ expressed in $Am^{-1}\,s^{-1}$. The values of C in our study are 3.5×10^9, 5.34×10^9, and 7.12×10^9 $Am^{-1}\,s^{-1}$ for the current 200, 300, and 400 A, respectively, used in the experiment. Thus, the amplitude of the magnetic field and frequency requirements are fulfilled in present study. It is also observed that an increment in the concentration of MNPs resulted in an increased value of optimal ΔT while decreased SAR, which suggests that increasing MNPs concentration to achieve optimal temperature is not an option to obtain a high value of SAR.

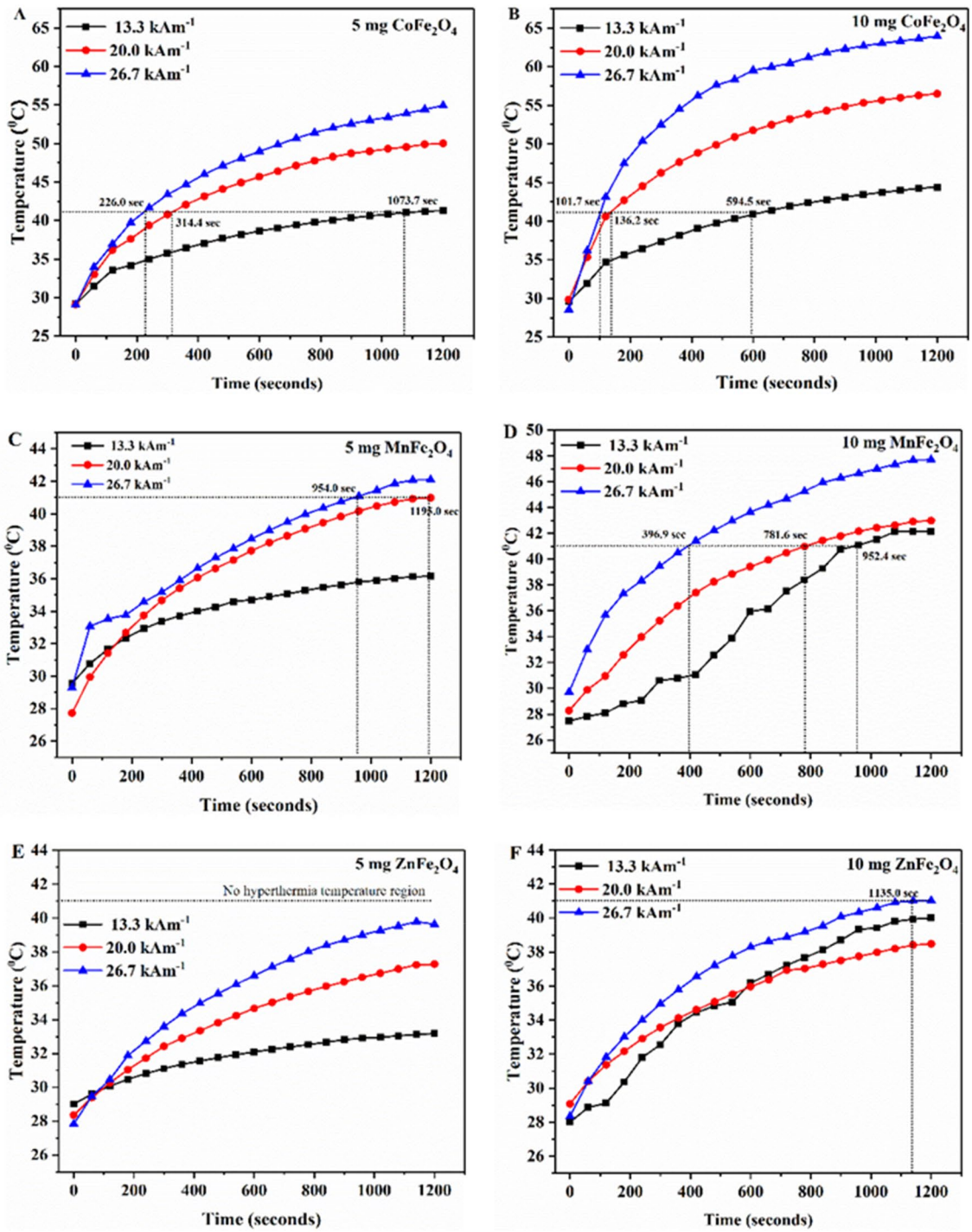

Fig. 4 Temperature verses time curves using 5 mgmL^{-1} **(A)** and 10 mgmL^{-1} **(B)** of $CoFe_2O_4$; 5 mgmL^{-1} **(C)** and 10 mgmL^{-1} **(D)** of $MnFe_2O_4$; and 5 mgmL^{-1} **(E)** and 10 mgmL^{-1} **(F)** of $ZnFe_2O_4$ MNPs at 13.3–26.7 kAm^{-1} field amplitude (*dotted line* indicates the hyperthermia temperature region)

To determine the applicability of SAR values obtained at different experimental parameters like a magnetic field, frequency, size, and concentration of MNPs, the alternate favorable term [16, 24], intrinsic loss power (ILP, in nHm^{2}kg^{-1}) (Eq. 4) measured in nano-Henrys m^2 per kg is used as SAR varies linearly with the frequency and quadratically with the amplitude of applied magnetic field and expressed as,

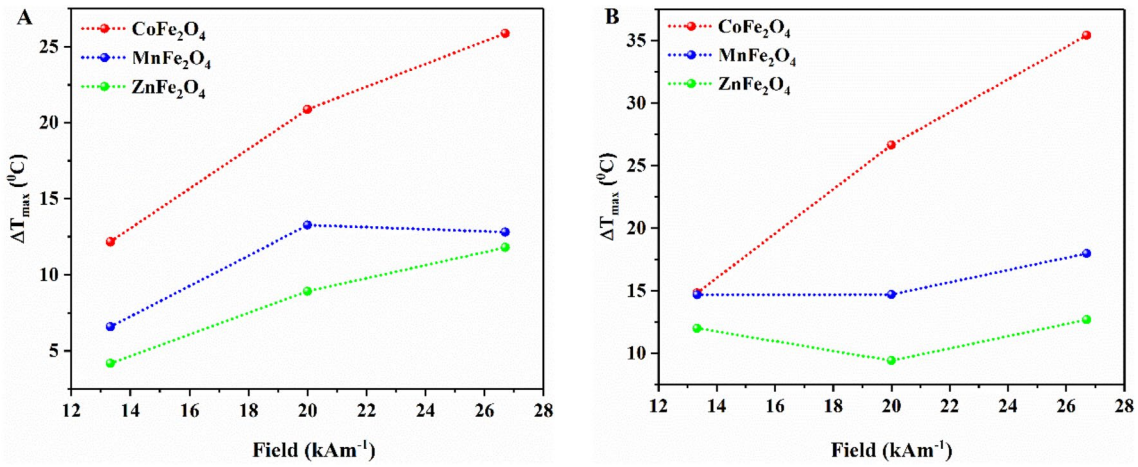

Fig. 5 Graphs showing the actual temperature rise (ΔT_{max}) obtained by $CoFe_2O_4$ (red), $MnFe_2O_4$ (blue) and $ZnFe_2O_4$ (green) using 5 mgmL^{-1} **(A)** and 10 mgmL^{-1} **(B)** MNPs concentration at 13.3–26.7 kAm^{-1} field amplitude

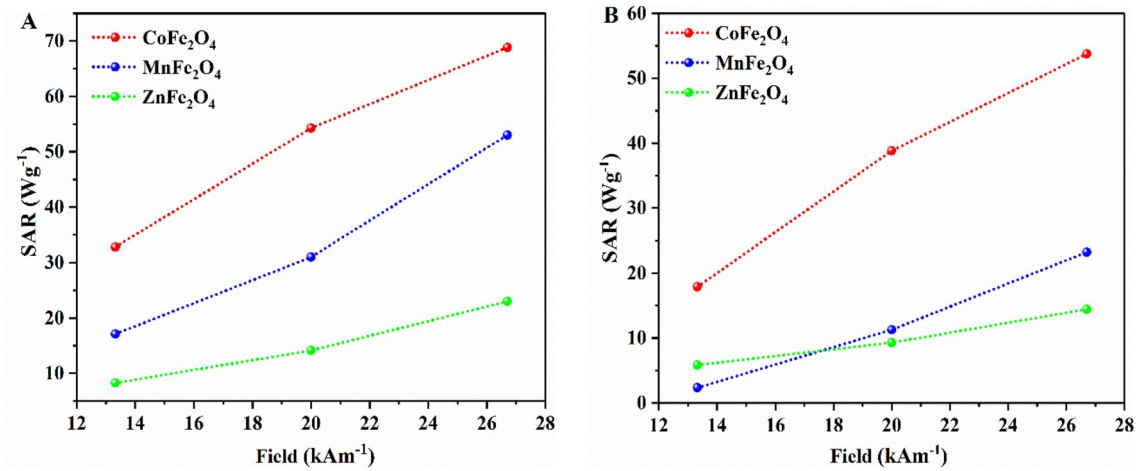

Fig. 6 Graphs showing obtained SAR values for $CoFe_2O_4$ (red), $MnFe_2O_4$ (blue), and $ZnFe_2O_4$ (green) using 5 mgmL^{-1} **(A)** and 10 mgmL^{-1} **(B)** MNPs concentration at 13.3–26.7 kAm^{-1} field amplitude

$$\mathrm{ILP}\left[n\mathrm{Hm}^2\mathrm{kg}^{-1}\right] = \frac{\mathrm{SAR}\left[W\mathrm{kg}^{-1}\right]}{f\left[\mathrm{kHz}\right]H^2\left[\left(\mathrm{kAm}^{-1}\right)^2\right]} \tag{4}$$

The frequency and the amplitude of magnetic field used in the experiments are accountable to find out the ILP values. The SAR value findings from our study were further treated using Eq. (4) to obtain the ILP values (Fig. 7). From the results, it indicates that the ILP values decrease with the increase in the MNPs concentration as well as the amplitude of the magnetic field. The maximum ILP value for $CoFe_2O_4$, $MnFe_2O_4$, and $ZnFe_2O_4$ was found to be at 5 mgmL^{-1} concentration and 13.32 kAm^{-1} field amplitude; while these values are, respectively, 0.67, 0.16, and 0.34 nHm^{2}kg^{-1}. The study finally reveals that out of the obtained MNPs by the present complex decomposition method, $CoFe_2O_4$ and $MnFe_2O_4$ show their applicability for MFH applications; while $ZnFe_2O_4$ is inefficient for this application due to the low internal hyperfine field.

4 Conclusion

The complex decomposition method employed is found to be efficient for the synthesis of superparamagnetic NPs with the particle size below 10 nm. The M-H curves, FTIR, Raman, and Mossbauer spectroscopy all played a vital role in determining the magneto-structural properties from which the formation of phase pure cubic spinel ferrite is confirmed. The MNPs were investigated in the

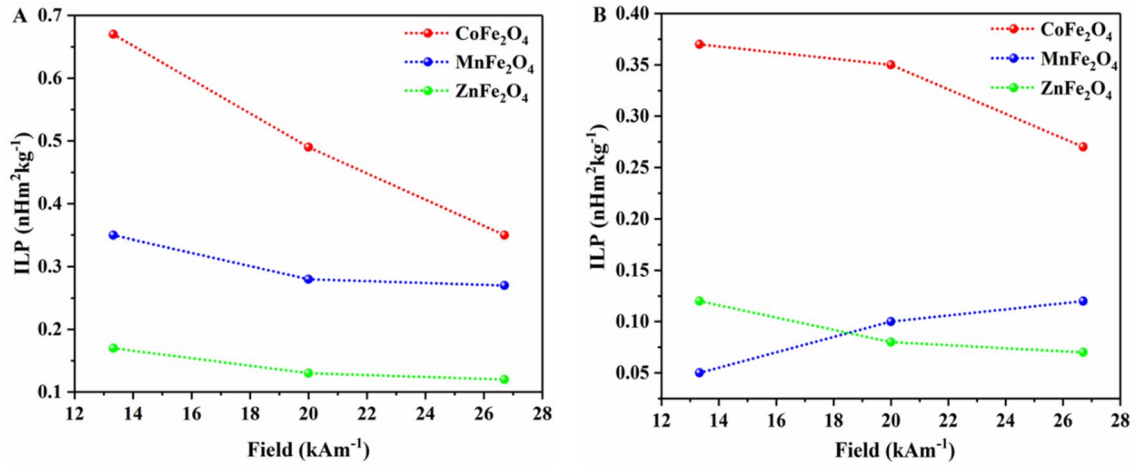

Fig. 7 Graphs showing obtained ILP values for $CoFe_2O_4$ (red), $MnFe_2O_4$ (blue) and $ZnFe_2O_4$ (green) using 5 $mgmL^{-1}$ **(A)** and 10 $mgmL^{-1}$ **(B)** MNPs concentration at 13.3–26.7 kAm^{-1} field amplitude

induction heating studies. We conclude that $CoFe_2O_4$ and $MnFe_2O_4$ have the potential for magnetic fluid hyperthermia as they offer rich threshold temperatures within the human tolerable range of frequency and amplitude of the applied magnetic field. The maximum ILP value for $CoFe_2O_4$ and $MnFe_2O_4$ was found to be 0.67 and 0.16 nHm^2kg^{-1}, respectively. In contrast, $ZnFe_2O_4$ fails to obtain the required threshold temperature under the same conditions, which may be ascribed due to the low average internal hyperfine field (H_f). Hence, the magneto-structural properties are directly allied to the induction heating properties of MNPs which can be manipulated by varying doping metal, size, and morphology of MNPs along with the synthesis method to make them potentially applicable for MFH. Further, more *in-vivo* and *in-vitro* studies of MNPs are suggested in order to ascertain the biocompatibility for applications in cancer treatment.

Acknowledgements Authors are grateful to the Department of Science & Technology, New Delhi, for the grants under DST-FIST program (No. SR/FST/college-151/2013 (C)) to Jaysingpur College, Jaysingpur. Authors are also thankful to the Indian Institute of Geomagnetism (IIGM), Panvel for characterization using AGM for magnetism as well as UGC-DAE Consortium for Scientific Research, Indore Centre for characterization using Raman and Mossbauer spectroscopy. Dr. X.-Y. Yu thanks for the support of the Pacific Northwest National Laboratory (PNNL). PNNL is operated for the U.S. Department of Energy by Battelle Memorial Institute under Contract No. DE-AC05-76RL01830.

Compliance with ethical standards

Conflict of interest The authors declare that they have no conflict of interest.

References

1. Iglesias D, Sabater S, Azua A, Mata JA (2015) Catalytic applications of magnetic nanoparticles functionalized using iridium N-heterocyclic carbene complexes. New J Chem 39:6437–6444. https://doi.org/10.1039/C5NJ00803D
2. Jadhav V, Chikode P, Nikam G, Sabale S (2016) Polyol synthesis and characterization of ZnO@ CoFe2O4 MNP's to study the photodegradation rate of azo and diphenyl type dye. Mater Today: Proc 3:4121–4127. https://doi.org/10.1016/j.matpr.2016.11.084
3. McNamara K, Tofail SA (2017) Nanoparticles in biomedical applications. AdvPhys: X 2:54–88. https://doi.org/10.1080/23746149.2016.1254570
4. Obaidat IM, Issa B, Haik Y (2015) Magnetic properties of magnetic nanoparticles for efficient hyperthermia. Nanomaterials 5:63–89. https://doi.org/10.3390/nano5010063
5. Sabale SR (2020) Studies on catalytic activity of MnFe2O4 and CoFe2O4MNPsas mediators in hemoglobin based biosensor. Mater Today: Proc 23:139–146. https://doi.org/10.1016/j.matpr.2020.02.011
6. Ban Q, Bai T, Duan X, Kong J (2017) Noninvasive photothermal cancer therapy nanoplatforms via integrating nanomaterials and functional polymers. BiomaterSci 5:190–210. https://doi.org/10.1039/C6BM00600K
7. Hergt R, Dutz S, Müller R, Zeisberger M (2006) Magnetic particle hyperthermia: nanoparticle magnetism and materials development for cancer therapy. J Phys: Condens Matter 18:S2919. https://doi.org/10.1088/0953-8984/18/38/S26
8. Sabale S, Kandesar P, Jadhav V et al (2017) Recent developments in the synthesis, properties, and biomedical applications of core/shell superparamagnetic iron oxide nanoparticles with gold. BiomaterSci 5:2212–2225. https://doi.org/10.1039/C7BM00723J
9. Shokrollahi H (2017) A review of the magnetic properties, synthesis methods and applications of maghemite. J MagnMagn Mater 426:74–81. https://doi.org/10.1016/j.jmmm.2016.11.033

10. Silva SM, Tavallaie R, Sandiford L et al (2016) Gold coated magnetic nanoparticles: from preparation to surface modification for analytical and biomedical applications. ChemCommun 52:7528–7540. https://doi.org/10.1039/C6CC03225G
11. McNamara K, Tofail SA (2015) Nanosystems: the use of nanoalloys, metallic, bimetallic, and magnetic nanoparticles in biomedical applications. PhysChemChemPhys 17:27981–27995. https://doi.org/10.1039/C5CP00831J
12. Moumen A, Fattouhi M, Abderrafi K et al (2019) Nickel colloid nanoparticles: synthesis, characterization, and magnetic properties. J ClustSci 30:581–588. https://doi.org/10.1007/s10876-019-01517-8
13. Sabale S, Jadhav V, Khot V et al (2015) Superparamagnetic MFe 2 O 4 (M= Ni Co, Zn, Mn) nanoparticles: synthesis, characterization, induction heating and cell viability studies for cancer hyperthermia applications. J Mater Sci - Mater Med 26:127. https://doi.org/10.1007/s10856-015-5466-7
14. You H, Yang S, Ding B, Yang H (2013) Synthesis of colloidal metal and metal alloy nanoparticles for electrochemical energy applications. ChemSoc Rev 42:2880–2904. https://doi.org/10.1039/C2CS35319A
15. Sadaqat A, Almessiere M, Slimani Y et al (2019) Structural, optical and magnetic properties of Tb3+ substituted Co nanoferrites prepared via sonochemical approach. Ceram Int 45:22538–22546. https://doi.org/10.1016/j.ceramint.2019.07.280
16. Behdadfar B, Kermanpur A, Sadeghi-Aliabadi H et al (2012) Synthesis of high intrinsic loss power aqueous ferrofluids of iron oxide nanoparticles by citric acid-assisted hydrothermal-reduction route. J Solid State Chem 187:20–26. https://doi.org/10.1016/j.jssc.2011.12.011
17. Jacintho GV, Brolo AG, Corio P et al (2009) Structural investigation of MFe2O4 (M= Fe, Co) magnetic fluids. J PhysChem C 113:7684–7691. https://doi.org/10.1021/jp9013477
18. Pereira C, Pereira AM, Fernandes C et al (2012) Superparamagnetic MFe2O4 (M= Fe Co, Mn) nanoparticles: tuning the particle size and magnetic properties through a novel one-step coprecipitation route. Chem Mater 24:1496–1504. https://doi.org/10.1021/cm300301c
19. Pradhan P, Giri J, Samanta G et al (2007) Comparative evaluation of heating ability and biocompatibility of different ferrite-based magnetic fluids for hyperthermia application. J Biomed Mater Res Part B: ApplBiomater: Off J SocBiomater, JpnSocBiomater, AustSocBiomater Korean SocBiomater 81:12–22. https://doi.org/10.1002/jbm.b.30630
20. Mohammad F, Balaji G, Weber A et al (2010) Influence of gold nanoshell on hyperthermia of superparamagnetic iron oxide nanoparticles. J PhysChem C 114:19194–19201. https://doi.org/10.1021/jp105807r
21. Yelenich O, Solopan S, Kolodiazhnyi T et al (2015) Magnetic properties and AC losses in AFe2O4 (A= Mn Co, Ni, Zn) nanoparticles synthesized from nonaqueous solution. J Chem. https://doi.org/10.1155/2015/532198
22. Bae S, Lee SW, Hirukawa A et al (2008) AC magnetic-field-induced heating and physical properties of ferrite nanoparticles for a hyperthermia agent in medicine. IEEE Trans Nanotechnol 8:86–94. https://doi.org/10.1109/TNANO.2008.2007214
23. Kim D-H, Nikles DE, Johnson DT, Brazel CS (2008) Heat generation of aqueously dispersed CoFe2O4 nanoparticles as heating agents for magnetically activated drug delivery and hyperthermia. J MagnMagn Mater 320:2390–2396. https://doi.org/10.1016/j.jmmm.2008.05.023
24. Wildeboer R, Southern P, Pankhurst Q (2014) On the reliable measurement of specific absorption rates and intrinsic loss parameters in magnetic hyperthermia materials. J Phys D ApplPhys 47:495003. https://doi.org/10.1088/0022-3727/47/49/495003
25. Semenova EM, Vorobyova SA, Lesnikovich AI et al (2012) Fabrication and investigation of magnetite nanoparticles with gold shell. J Alloy Compd 530:97–101. https://doi.org/10.1016/j.jallcom.2012.03.090
26. Bao N, Shen L, Wang Y et al (2007) A facile thermolysis route to monodisperse ferrite nanocrystals. J Am ChemSoc 129:12374–12375. https://doi.org/10.1021/ja074458d
27. Herrera AP, Polo-Corrales L, Chavez E et al (2013) Influence of aging time of oleate precursor on the magnetic relaxation of cobalt ferrite nanoparticles synthesized by the thermal decomposition method. J MagnMagn Mater 328:41–52. https://doi.org/10.1016/j.jmmm.2012.09.069
28. Park J, An K, Hwang Y et al (2004) Ultra-large-scale syntheses of monodisperse nanocrystals. Nat Mater 3:891–895. https://doi.org/10.1038/nmat1251
29. Sabale S, Jadhav V, Mane-Gavade S, Yu X-Y (2019) Superparamagnetic CoFe 2 O 4@ Au with high specific absorption rate and intrinsic loss power for magnetic fluid hyperthermia applications. ActaMetallurgicaSinica (English Letters) 32:719–725. https://doi.org/10.1007/s40195-018-0830-5
30. Li X-H, Xu C-L, Han X-H et al (2010) Synthesis and magnetic properties of nearly monodisperse CoFe 2 O 4 nanoparticles through a simple hydrothermal condition. Nanoscale Res Lett 5:1039–1044. https://doi.org/10.1007/s11671-010-9599-9
31. Panda N, Sahu D, Acharya B et al (2014) Effect of Zn concentration on microstructural, optical, and hyperfine properties of nanocrystalline α-Fe 2 O 3. ActaMetallurgicaSinica (English Letters) 27:563–568. https://doi.org/10.1007/s40195-014-0093-8
32. Tatarchuk T, Shyichuk A, Trawczyńska I et al (2020) Spinel cobalt (II) ferrite-chromites as catalysts for H2O2 decomposition: synthesis, morphology, cation distribution and antistructure model of active centers formation. Ceram Int 46:27517–27530. https://doi.org/10.1016/j.ceramint.2020.07.243
33. Gandha K, Elkins K, Poudyal N, Ping Liu J (2015) Synthesis and characterization of CoFe2O4 nanoparticles with high coercivity. J ApplPhys 117:17A736. https://doi.org/10.1063/1.4916544
34. Shemer G, Tirosh E, Livneh T, Markovich G (2007) Tuning a colloidal synthesis to control Co2+ doping in ferrite nanocrystals. J PhysChem C 111:14334–14338. https://doi.org/10.1021/jp076793
35. Rafique MY, Li-Qing P, Iqbal MZ et al (2013) Growth of monodisperse nanospheres of MnFe2O4 with enhanced magnetic and optical properties. Chin Phys B 22:107101. https://doi.org/10.1088/1674-1056/22/10/107101
36. Wang Z, Schiferl D, Zhao Y, O'Neill HSC (2003) High pressure Raman spectroscopy of spinel-type ferrite ZnFe2O4. J PhysChem Solids 64:2517–2523. https://doi.org/10.1016/j.jpcs.2003.08.005
37. Andrade PL, Silva VAJ, Maciel JC et al (2014) Preparation and characterization of cobalt ferrite nanoparticles coated with fucan and oleic acid. Hyperfine Interact 224:217–225. https://doi.org/10.1007/s10751-013-0835-4
38. Li Y, Jiang J, Zhao J (2004) X-ray diffraction and Mössbauer studies of phase transformation in manganese ferrite prepared by combustion synthesis method. Mater ChemPhys 87:91–95. https://doi.org/10.1016/j.matchemphys.2004.05.007
39. Yang A, Chinnasamy C, Greneche J et al (2009) Enhanced neel temperature in Mn ferrite nanoparticles linked to growth-rate-induced cation inversion. Nanotechnology 20:185704. https://doi.org/10.1088/0957-4484/20/18/185704
40. Battle J, Clark T, Evans B (1997) 57Fe Mössbauer spectroscopy of zinc ferrite prepared by a variety of synthetic methods. Le Journal de Physique IV 7:C1-257. https://doi.org/10.1051/jp4:1997199
41. Rajendran M, Pullar R, Bhattacharya A et al (2001) Magnetic properties of nanocrystalline CoFe2O4 powders prepared at room temperature: variation with crystallite size. J MagnMagn

Mater 232:71–83. https://doi.org/10.1016/S0304-8853(01)00151-2
42. Périgo EA, Hemery G, Sandre O et al (2015) Fundamentals and advances in magnetic hyperthermia. ApplPhys Rev 2:041302. https://doi.org/10.1063/1.4935688
43. Levy M, Quarta A, Espinosa A et al (2011) Correlating magneto-structural properties to hyperthermia performance of highly monodisperse iron oxide nanoparticles prepared by a seeded-growth route. Chem Mater 23:4170–4180. https://doi.org/10.1021/cm201078f